Desalination 613 (2025) 119023

Contents lists available at ScienceDirect

Desalination

journal homepage: www.elsevier.com/locate/desal

Incipient $CaCO_3$-scaling detection for scaling mitigation

Martin Futterlieb [a,*], Stefan Panglisch [a,b,c,d]

[a] University of Duisburg-Essen, Lotharstr. 1, 47057 Duisburg, Germany
[b] Center for Water and Environmental Research (ZWU), Universitätsstraße 2, 45141 Essen, Germany
[c] IWW Water Center, Moritzstraße 26, 45476 Mülheim an der Ruhr, Germany
[d] DGMT German Society of Membrane Technology, Geschäftsstelle ZWU, Universitätsstraße 2, 45141 Essen, Germany

HIGHLIGHTS

- Early $CaCO_3$-scaling detection via concentrate-pH before permeability drop
- Concentrate-pH enables operation at scaling threshold without antiscalants
- Conductivity and turbidity are slower or less reliable scaling indicators
- Water chemistry simulations unraveled the delayed conductivity drop
- Permeability drop is masked by concentration polarization

GRAPHICAL ABSTRACT

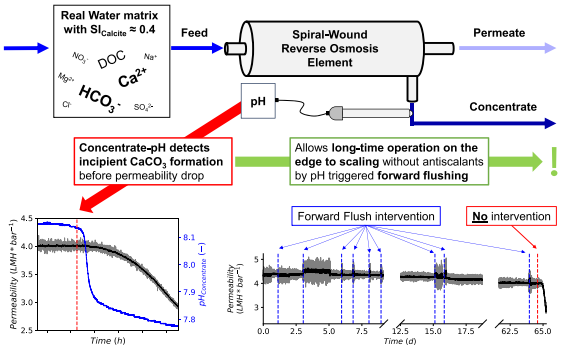

ARTICLE INFO

Keywords:
Reverse osmosis
$CaCO_3$-scaling
Scaling mitigation
Early scaling detection

ABSTRACT

The formation of scale deposits on the membrane surface due to the precipitation of sparingly soluble salts is a major obstacle limiting the recovery of inland membrane desalination. A simple approach to mitigating scaling is its early detection, allowing for timely countermeasures. Early scaling detection is mainly limited to laboratory studies with flat sheet membranes and synthetic feedwaters using sophisticated detection tools. This impedes transferability to an industrial scale, where spiral-wound elements are commonly used. The present study advances the previous research using pilot and laboratory-scale spiral-wound elements and a real water matrix. It demonstrates that monitoring changes in concentrate quality is an effective and practical way to detect incipient $CaCO_3$ scaling. It was found that the concentrate-pH is a reliable indicator that recognizes incipient $CaCO_3$ formation well before a scaling-induced drop in permeability. By monitoring concentrate pH in real time, countermeasures such as forward flushing can be triggered in a timely manner to reliably prevent $CaCO_3$ scaling. This allowed stable operation near the onset of scaling (calcite saturation index of 1.7 to 2.0) even without dosing an antiscalant for over two months. Forward flushing not only removed the concentration polarization layer but also led to the dissolution of $CaCO_3$ deposits that had already formed. This shows for the first time that incipient $CaCO_3$ scale deposits are reversible if intervention is carried out in time. Moreover, water chemistry models and simulations were conducted to gain a deeper understanding of the underlying mechanisms, particularly regarding the late response of the permeability and conductivity.

* Corresponding author.
E-mail addresses: martin.futterlieb@uni-due.de (M. Futterlieb), stefan.panglisch@uni-due.de (S. Panglisch).

https://doi.org/10.1016/j.desal.2025.119023
Received 15 December 2024; Received in revised form 28 April 2025; Accepted 15 May 2025
Available online 17 May 2025

1. Introduction

Pressure-driven dense membrane filtration (i.e., reverse osmosis (RO) and nanofiltration (NF)) is deployed in inland locations to supply potable or process water from conventional freshwater resources, like surface- [1,2] and groundwater [3–5]. Moreover, dense membranes are the core technology to provide water from unconventional resources, such as brackish water, treated wastewater effluents [6,7], and agriculture runoffs [8,9]. Typical treatment objectives range from full desalination to targeted or combined removal of hardness [3,5,10], sulphate [8,11,12], nitrate [4], chloride, organic matter [1,2], and micropollutants [13], such as PFAS [2,14,15] and pesticides [1]. A significant bottleneck of inland desalination is the disposal of the concentrated waste stream (i.e., brine) [16,17], which is the main cost driver [18] and associated with environmental concerns [19]. Subsequently, a high recovery is required to minimize the brine flow and ensure economic operation [17,20,21], which might be additionally demanded due to limited water extraction rights. However, the recovery is usually constrained by the occurrence of membrane scaling [18,22].

Membrane scaling is the precipitation of supersaturated sparingly soluble salts, such as calcium carbonate ($CaCO_3$) [23–26], calcium sulfate ($CaSO_4$) [8,9,11,27], silica (SiO_2) [28] or calcium phosphate, e.g., as hydroxyapatite ($Ca_5(PO_4)_3OH$) [20,29,30] onto the membrane [31–33]. Membrane scaling reduces the permeability [31,32,34] due to the formation of a dense mineral layer with a high hydraulic resistance [31] and will lead, depending on the mode of operation, either as constant pressure or constant flux, to lowered product water (permeate) quantity or higher necessary applied pressure, respectively. The mineral layer will additionally increase the hydraulic pressure drop [33]. Moreover, the salt passage increases [35], which leads to lowered permeate quality [31]. Lastly, scaling increases cleaning intervals and shortens the lifetime of the membranes [31,34,35]. Therefore, scaling needs to be prevented.

Although there are different options to reduce the likelihood of scaling, the most common scale control method is the dosage of antiscalants [10,34,36]. Antiscalants are synthetic organic polyelectrolytes, such as polyphosphonates and polycarboxylates, impurities that inhibit the crystallization process at below-stoichiometry concentrations [36,37]. However, the application of antiscalants comes with certain drawbacks. For once, purchasing the antiscalants creates additional operating costs [2,36]. Furthermore, the discharge of brine-bearing antiscalants is associated with environmental concerns [16,32], particularly in inland locations [19]. Moreover, antiscalants can be detected in the permeate [38], raising public health concerns. Antiscalants might furthermore promote biofouling [39,40]. The study of Mangal et al. [26] showed that overdosing of commercial phosphonate-based antiscalants applied to prevent $CaCO_3$-scaling can lead to the formation of calcium-antiscalant compounds, e.g., calcium-phosphonates, which build a fouling layer. Certain water constituents, such as iron and manganese, may adversely influence the effect of antiscalants [10], and some research reported that the dosage of antiscalants did not show any gain in the maximum attainable recovery compared to no antiscalants dosage [41].

Pre-treatment schemes to remove or reduce scaling ions (e.g., calcium) are other measures to prevent membrane scaling. Possible options are, e.g., ion exchange [42–44] or precipitation [45]. Moreover, membrane modification, e.g., by surface patterning [46], increasing membrane hydrophilicity [47], and modifying surface charges [29,30], may increase scaling resistance. Adjusting the mode of operation, e.g., discontinuous operation as batch or semi-batch [48,49], as well as flow reversal [50–52], showed further potential to mitigate scaling.

A simple and effective scaling-mitigation strategy would be a reliable detection method to identify specific scaling at an early stage before any performance loss can be detected. This would enable the initiation of appropriate countermeasures to reduce the impact of the deposits or even entirely prevent them altogether, e.g. by improving the cleaning strategy. Typically, it is assumed that bulk measurements and conventional parameters, e.g., permeability, lack sensitivity to detect scaling at an early stage [53,54]. Therefore, in literature, sophisticated detection tools, e.g., ultrasonic reflectometry [55] or electrical impedance spectroscopy [53,54] are examined. Various studies investigated early scaling detection, focussing on optical observation of transparent cells for early scaling detection [56–61].

Bartman et al. [56] detected the first deposits of $CaSO_4$-minerals before the permeability significantly decreased (< 5 %) using a transparent RO-cell observed with real-time imagining. Supekar et al. [58] applied Raman spectroscopy to detect $CaSO_4$-scaling within a flow cell. The earliest detection of $CaSO_4$ was indicated by an increase in peak intensity at a decrease of 3.2 % in permeate flow rate [58]. Raman spectroscopy allows distinguishing between different scalants [58] facilitating subsequent cleaning strategies. However, applying flow cells for incipient scaling detection [56,58] has certain drawbacks. For once, the hydrodynamics of spiral-wound elements differ from those of the deployed flat-sheet membranes, presumably restricting transferability [8]. Moreover, typically, only a small section is observed, potentially missing other nascent nuclei-cluster [8].

Interestingly, already in 2000, van de Lisdonk et al. [62] showed a comparable simple possibility of early scaling detection using an additional membrane element (“ScaleGuard”) fed with RO-concentrate from a full-scale installation. Due to the slightly higher recovery (1 to 4 % increase compared to the last element) and the monitoring of a single element compared to monitoring a six-element pressure vessel, the scaling monitor could successfully detect scaling before it occurred in the last element of the full-scale installation [62]. Recently Schwiebert et al. [8] presented a practical and straightforward method for early scaling detection using bulk concentrate turbidity measurement. The study showed prevention of $CaCO_3$- and $CaSO_4$-scaling using turbidity to detect incipient scaling for a synthetic agriculture run-off solution treated with batch-RO [8].

This study addresses significant research gaps by investigating $CaCO_3$ scaling using both pilot and lab-scale spiral-wound elements with a real water matrix. In contrast to conventional approaches based on flat sheet membranes and synthetic, already highly concentrated feedwaters, this study uses a continuous flow reflecting real-world conditions.

The study uses standard equipment to monitor key membrane parameters such as permeability, salt retention, and pressure loss, as well as quality measurements in the bulk concentrate like pH, electrical conductivity (EC), and turbidity. By using a real water matrix, the study tackles complex challenges such as multiple scalants and combined fouling due to organic constituents.

The objectives of this research are, (i) to assess the impact of $CaCO_3$ scaling on standard scaling parameters; (ii) to identify a suitable parameter for early $CaCO_3$ scaling detection; (iii) to evaluate the feasibility of this parameter as an early warning signal in long-term experiments; (iv) to develop models and simulations explaining the observed results. This approach enhances the transferability of findings to practical applications, providing valuable insights into mitigating scaling in membrane desalination.

2. Theoretical background

To facilitate the interpretation of the later presented results, general basics of crystal formation and in particular on $CaCO_3$-precipitation are outlined in this chapter.

2.1. Basics of crystallization

Scale formation starts with nucleation, i.e., the transformation from an ion-containing solution to a new thermodynamic solid phase [32] by clustering of ion pairs to pre-nuclei from about 1000 atoms [63], followed by an ordering step to larger nuclei (>3 nm), which collectively describes nucleation [64]. Nucleation is a reversible process, i.e., nuclei

may grow further or dissolve until a critical nuclei or cluster size is reached [63,64]. After reaching a critical nucleus size, further growth yields in crystals larger than 100 nm [63], i.e., the crystal growth phase. Nucleation, i.e., the nascent stage of crystal precipitation [65], can be described thermodynamically, with the difference of chemical potential ($\Delta\mu$) as the driving force for nucleation [32]. Since mass transfer is always from high to low chemical potential, the solutions' chemical potential in nuclei formation is higher than the solids' potential [32]. The saturation index (*SI*) is often used to describe the chemical potential of the solution and the solid. The saturation index is the decadic logarithm fraction of the ion activity product (*IAP*) to the solubility product (K_{SP}) of the respective ions and salt [66]:

$$SI = log_{10}\frac{IAP}{K_{SP}} \quad (1)$$

Other forms describing the saturation index are possible, e.g., as a natural logarithmic form [32,64] or even in non-logarithmic forms. Therefore, caution is needed when comparing different SIs from literature. However, for all forms of saturation indices, the following applies: If the $IAP > K_{SP,}$ the solution is oversaturated (or supersaturated) [64]. In the case of $IAP = K_{SP,}$ the solution is in equilibrium, while when $IAP < K_{SP,}$ the solution is undersaturated [64]. Therefore, the formation of nuclei, i.e., membrane-scaling, is possible from a thermodynamic point of view at a supersaturated state.

In general, nuclei formation is distinguished into homogenous and heterogenous pathways [67]. Homogenous nucleation describes nuclei formation from a bulk solution, whereas heterogenous nucleation includes additional (solid) surfaces [64,67]. Thermodynamically, heterogeneous nucleation is more favorable since the interfacial energy between the additional surface and the nuclei is reduced compared to bulk nucleation, i.e., interfacial energy between the nuclei and the solution [64]. Therefore, surfaces lower the threshold difference in chemical potential, i.e., saturation index, for nucleation [64]. Relating the fundamentals of nucleation on membrane scaling leads to a differentiation between bulk (homogenous) and surface (heterogenous) driven scale formation in membrane processes [27,34,68,69]. For homogenous scale formation, crystals are formed within the bulk and deposit onto the membrane, while in heterogenous surface formation, nuclei form directly on the membrane [69]. However, heterogeneous nucleation is not necessarily triggered at the membrane surface. Suspended particles within the bulk can act as surface, too, leading to heterogenous nucleation within the bulk [23,70]. Typically, homogenous nucleation is predominant at high supersaturation, whereas heterogenous nucleation is expected at lower supersaturation [71]. Benecke et al. [11] summarized studies suggesting either homogenous, heterogenous or their combination as cause of scale formation.

Besides thermodynamic considerations, i.e., saturation indices, kinetics play an essential role, too. Although analyzing the susceptible water allows us to compute the respective saturation, it gives no information about the stability of a supersaturated solution [24]. This means that a supersaturated solution does not necessarily lead to precipitation on a technical scale but that a certain elapsed time or a minimum supersaturation is necessary. The elapsed time from reaching a supersaturated state until a (measurable) physical change of the solution is labelled, among other things, as nucleation or induction time, experimental induction period or crystallization induction time [50,72–74]. The longer it takes to see a measurable change, i.e., the longer the induction time, the less likely is the occurrence of membrane scaling [74]. The induction time depends on the method of detection [65], which covers a wide range, e.g., the appearance of visible crystals, decrease of the conductivity in the solution, an increase in turbidity [72,73] or for carbonate salts a dropping pH [24], see chapter 2.2. However, Mitrouli et al. [23] suggested that the concept of induction time does not apply to technical systems, arguing that the inevitable presence of particles promotes heterogenous nucleation, drastically lowering the induction time to an unmeasurable level, as demonstrated in their study for $CaCO_3$-scaling.

2.2. $CaCO_3$-precipitation

Calcium carbonate- ($CaCO_3$) precipitation is one of the most relevant scalants in dense membrane filtration [34,70,75]. The formation of $CaCO_3$ is a multiple-chemical reaction involving all inorganic carbon species, i.e., CO_2/H_2CO_3, HCO_3^-, CO_3^{2-}. The reaction involves in total four partial reactions which can be summed up to Eq. (2) [64]:

$$Ca^{2+} + 2HCO_3^- \leftrightarrow CaCO_3(s) + CO_2(g) + H_2O \quad (2)$$

Eq. (2) shows that the precipitation of 1 mol $CaCO_3$ consumes 1 mol of Ca^{2+} and 2 mols of HCO_3^-. As known for all types of scalants, their precipitation will thus lead to lower electrical conductivity (EC) since dissolved constituents are transformed into a solid, leading to increased turbidity due to increased particle concentration. However, special about $CaCO_3$-scaling is the release of CO_2 and consumption of HCO_3^-. Therefore, precipitation will decrease the pH, and consequently, the dissolution of $CaCO_3$ will increase the pH. Thus, the pH can be used to identify and to measure the induction time of $CaCO_3$ precipitation [24,74]. The study of Waly et al. [24] defined a drop of at least 0.03 pH units as reaching the induction time.

The solubility of $CaCO_3$ decreases with increasing temperature and pH. Therefore, an increase in recovery not only increases the ion activity product, as with all other sparingly soluble salts, but also increases the concentrate-pH, thus reducing the $CaCO_3$-solubility and shifting the total inorganic carbon (TIC) fractions to HCO_3^- and CO_3^{2-}, and consequently increasing the supersaturation of $CaCO_3$. Due to this pH dependency, lowering the pH, e.g., purging of CO_2 [76] and thus increasing the $CaCO_3$-solubility, is an effective measure to minimize $CaCO_3$-scaling [31].

In general, the solubility of $CaCO_3$ is significantly lower than that of other sparingly soluble salts, e.g., $CaSO_4$ [31]. There are various forms of $CaCO_3$-minerals. However, the most stable form is the cubical-shaped calcite, i.e., having the lowest solubility product [31].

3. Material and methods

3.1. Feed water, experimental equipment and procedure

In all experiments, the plants were continuously fed with potable water (supply area North of Duisburg [77]). The water is supersaturated with calcite, with an average $SI_{Calcite}$ value of approximately 0.4. The saturation indices (SI) were calculated using PhreeqC (Version 3.1 with database PHREEQC.DAT [66]) following Eq. (1). Detailed analyses of the feedwater are summarized in chapter 1.1 of the Supplementary Information.

Within the study, two different plants were operated (Fig. 1). The fully automated four inch (4″) pilot plant (4″ represents the diameter of the used membrane elements), depicted in Fig. 1 a) to c), was built by the company Cornelsen Umwelttechnologie GmbH (Essen, Germany). The plant is equipped with two 4″ spiral-wound Suez-AK elements [78] in series (15.8 m^2 installed membrane surface). It should be noted that the AK series is now distributed by Veolia; see [79]. The plant was operated in feed and bleed mode, i.e., with constant concentrate recirculation and discharge, to achieve high recoveries with a single-stage design. A recirculation pump (RCP) (PN-SNA Grundfos) was integrated to operate with an internal recirculation loop. The high-pressure pump (HP) is a positive displacement pump (BN 1–24 Seepex/Ingersoll Rand). In all streams, pressure and flowmeters are integrated (not depicted in Fig. 1), e.g., to determine permeate flux (J_P), transmembrane pressure (*TMP*), pressure loss (Δp) and permeability (*P*). The quality parameters pH, EC, turbidity and temperature are monitored online in the feed- and in the concentrate stream. In addition, the permeate-EC (EC_P) is monitored to determine the EC-retention. In the internal recirculation line, EC is

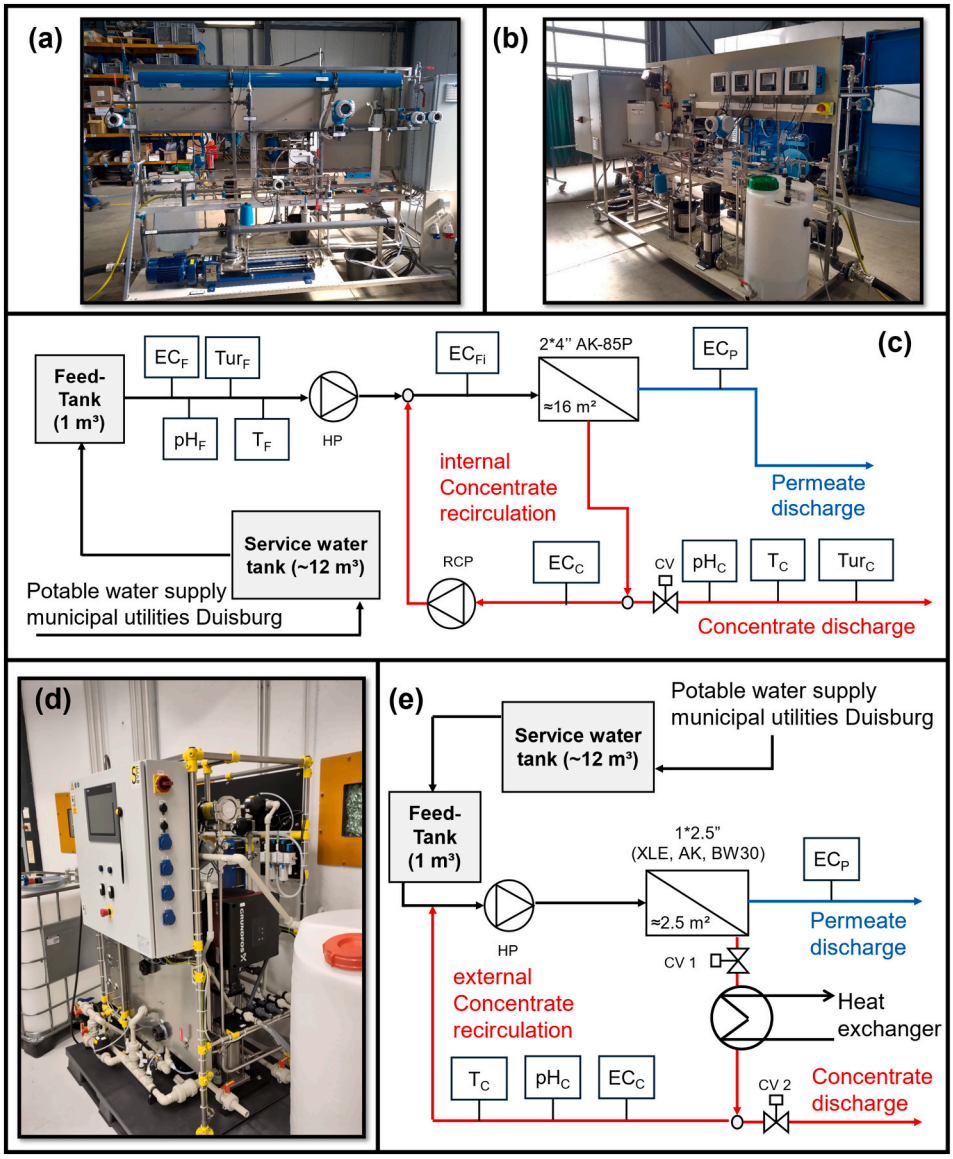

Fig. 1. Membrane plants: a) to c) 4″ pilot plant and 2.5″ lab plant (d and e). Simplified P&IDs (c and e) display only the quality measurements.

monitored online for the concentrate (EC_C) and the inner feed ($EC_{F,i}$). All measuring equipment was supplied by Endress+Hauser GmbH+*Co* KG.

Fig. 1 d) and e) depict the 2.5″ lab plant. The fully automated plant was built by the company SIMA- tec GmbH (Schwalmtal, Germany). The 2.5″ plant is equipped with one 2.5″ spiral-wound element. In total, three different membranes were used - the XLE 240 Pro (2.6 m^2) [80], the BW30 Pro 2540 (2.6 m^2) [81], both from DuPont and the Veolia AK2540 TM membrane (2.5 m^2) [79]. The 2.5″ plant was operated in feed and bleed with external concentrate recirculation since it is equipped with a single HP pump (CRNE-HS, Grundfos). A detailed list of the devices for quality measurements for the 4″ and 2.5″ plant can be found in Table S6 (Supplementary Information).

All experiments were operated at constant flux and constant concentrate discharge flow, resulting in a constant recovery. The crossflow velocity in the 4″ plant was set from 0.1 m/s to 0.071 m/s from the front of the first to the back of the second element. System related, the crossflow for the 2.5″ plant was higher with 0.135 to 0.127 m/s from front to the back of the single element. This velocities were adjusted to reflect real conditions in full-scale operation, as e.g., reported in Vrouwenvelder et al. [82].

Table 1 summarizes the experiments conducted and their numbering in the paper. In this study, the term LMH is used as the unit of displayed fluxes and is a short form of $\left(L/m^2*h\right)$. No antiscalants were applied in any of the experiments.

New membranes were first rinsed for 2 h with potable water, then operated at recoveries without risk of scaling and different fluxes for compaction. Thereafter, the membranes were operated for a minimum of 48 h at recoveries without any risk of scaling. The flux was adjusted to the respective flux of the subsequent scaling experiments (20 to 35 LMH), while permeability and salt-retention were monitored to evaluate whether compaction had been completed. After each scaling experiment, the plants, including the elements were cleaned. Depending on the severeness, the cleaning protocol included forward flushing and acid-alkali-acid chemical cleaning in place (CIP). Following each cleaning step, permeability and salt-retention were determined to evaluate the cleaning success. The cleaning protocol is described in detail in chapter 1.3 of the Supplementary Information.

3.2. Lab analysis

Relevant cations (Ca^{2+}, Mg^{2+}, Na^{+}) and anions (SO_4^{2-}, Cl^{-}, NO_3^{-})

Table 1
List of experiments.

Plant	Experiment ID	Operation mode		Membrane
		Flux (LMH)	Recovery	
4″ plant	4″(1)	20	90 %	AK85-P (Suez/Veolia)
	4″(2)	23	90 %	
2.5″ plant	2.5″(1)	35	85 %	XLE (DuPont)
	2.5″(2)	25	85 % for 33.8 days then increased to 90 %	AK (Veolia)
	2.5″(3)	28	Increased from 85 to 92 %	
	2.5″(4)	20	82.5 %	BW30 (DuPont)
	2.5″(5)	20	Different recoveries (75 to 82.5 %) with concentrate-pH triggered forward flush	

*The double prime mark (") represents the unit inch and displays the diameter of the used membrane elements with 2.5" and 4″ representing roughly 6.4 and 10.2 cm, respectively. LMH is an abbreviation for L/(m²*h) displaying the permeate flux. Experiment 4″(2) and 2.5″(3) are provided in the Supplementary Information, chapter 2.1 and 2.4.*

were analyzed using ion chromatography. Moreover, organic carbon, in the form of dissolved organic carbon (DOC), inorganic carbon as total inorganic carbon (TIC) as well as HCO_3^- were determined. Selected precipitates were analyzed with scanning electron microscopy with energy dispersive X-ray spectroscopy (SEM-EDX). Furthermore, electrical conductivity (EC) and pH were determined via handheld devices, when samples were collected from the plants. Detailed information about lab analysis are summarized in the Supplementary Information chapter 1.2.

3.3. Calculations

The permeability was corrected by the temperature and the osmotic pressure (π). Temperature correction functions (TCF) are membrane-specific and were obtained from the specific membrane supplier; see [33]. Correction for osmotic pressure of bulk and permeate was conducted based on the measured EC with:

$$\pi_{Bulk} = \frac{EC_{bulk}{}^{1.04} \cdot (T + 320)}{925.000} \tag{3}$$

T represents the temperature in °C. EC_{bulk} is the arithmetic mean of the inner feed ($EC_{F,i}$) and the concentrate (EC_C). In the case of the 2.5″ plant only the concentrate conductivity was online monitored, and the inner recovery was relatively low. Thus, it can be assumed that EC_C is approximately EC_{bulk}. The permeate osmotic pressure was calculated with EC_{Perm}. The transmembrane osmotic pressure (TMπ) was calculated by:

$$TM\pi = \pi_{bulk} - \pi_{Perm.} \tag{4}$$

The temperature and osmotic pressure corrected permeability can thus be calculated applying Eq. (5):

$$P_C = \frac{Q_P * A_M{}^{-1} * TCF}{TMP - TM\pi} = \frac{J_P * TCF}{TMP - TM\pi} \tag{5}$$

Q_P is the volumetric permeate flow, A_M the membrane surface and J_P the permeate flux. The term $(TMP - TM\pi)$ is the net transmembrane pressure available for the permeate transport through the membrane.

Further on, corrected permeabilities were occasionally normalized to a reference permeability ($P_{C,N}$). Unless otherwise described, the reference point was set when the EC retention stopped increasing in the respective experiment (after the membrane has been compacted, stable salt retention and permeability are achieved). Concentrate-pH and -EC were occasionally normalized, too. In this case, the reference point was set when the system reached a steady state, i.e., a constant pH and EC or their maximum values were achieved (see example in Fig. S4 in the Supplementary Information).

Additionally, the permeability ($P_{C,\beta}$) considering concentration polarization (CP) was calculated. The CP-factor β which represents the relation of the membrane concentration (c_M) to the bulk concentration (c_{Bulk}), was integrated:

$$P_{C,\beta} = \frac{J_P * TCF}{TMP - \beta * TM\pi} \tag{6}$$

The bulk retention was calculated by Eq. (7).

$$Rej._{EC,bulk} = 100\% * \left(1 - \frac{EC_{Perm.}}{EC_{bulk}}\right) \tag{7}$$

The hydraulic pressure loss between feed and concentrate was determined based on the differential pressure between the inlet of the pressure vessel and the outlet of the pressure vessel.

Data analysis was performed using Python 3 scripts within the web application Jupyter Notebook. Used functions are summarized in chapter 1.4 of the Supplementary Information.

Error analysis considered systematic errors by comparison of sample-values with known standard solutions and the accuracy of measurements was assessed on the basis of mass balances. Detailed information regarding the error analysis can be found in chapter 1.4 of the Supplementary Information.

3.4. Water chemistry model and simulations

A PhreeqC (Version 3.1 with database PHREEQC.DAT) model was created based on the concentrate composition of Experiment 4″(1) before scaling was observed. The model was used to investigate dynamic changes experienced due to $CaCO_3$-precipitation in three simulations. In Simulation 1 the influence of changing pH on the distribution of species and the conductivity was investigated, simulating pH-values between 7.2 and 9.2. In Simulation 2, in total 2 mM of CO_2 were added to the solution in 1000 steps using the reaction term. Finally, seven points in time shortly before and during the scaling event of Experiment 4″(1) were selected in Simulation 3 to simulate the behavior of the concentrate while $CaCO_3$ precipitation. Precipitation of $CaCO_3$ was simulated by forcing the solution to reach certain saturation indices of calcite ($SI_{Calcite}$) using the equilibrium phases term. The respective $SI_{Calcite}$ was iterated based on the measured concentrate-pH. Detailed information can be found in chapter 3 of the Supplementary Information.

4. Results and discussion

4.1. Scaling detection

Fig. 2 depicts a $CaCO_3$-scaling event in Experiment 4″(1), starting approximately after 30 h of operation. Initially, the permeability decreased slightly (linear fit yellow dashed line) and stabilized over time (grey dashed line), see Fig. 2 a). The scaling event is characterized by a dropping permeability (red dashed line) and a decreasing concentrate-pH and -conductivity (EC), see Fig. 2 b). Interestingly, a decrease in concentrate-pH and -EC was accompanied by an increase in permeability, which persisted for approximately one and a half hours (blue dashed line) before it began to decline again (red dashed line). It took nearly four hours for the permeability to drop below its initial value

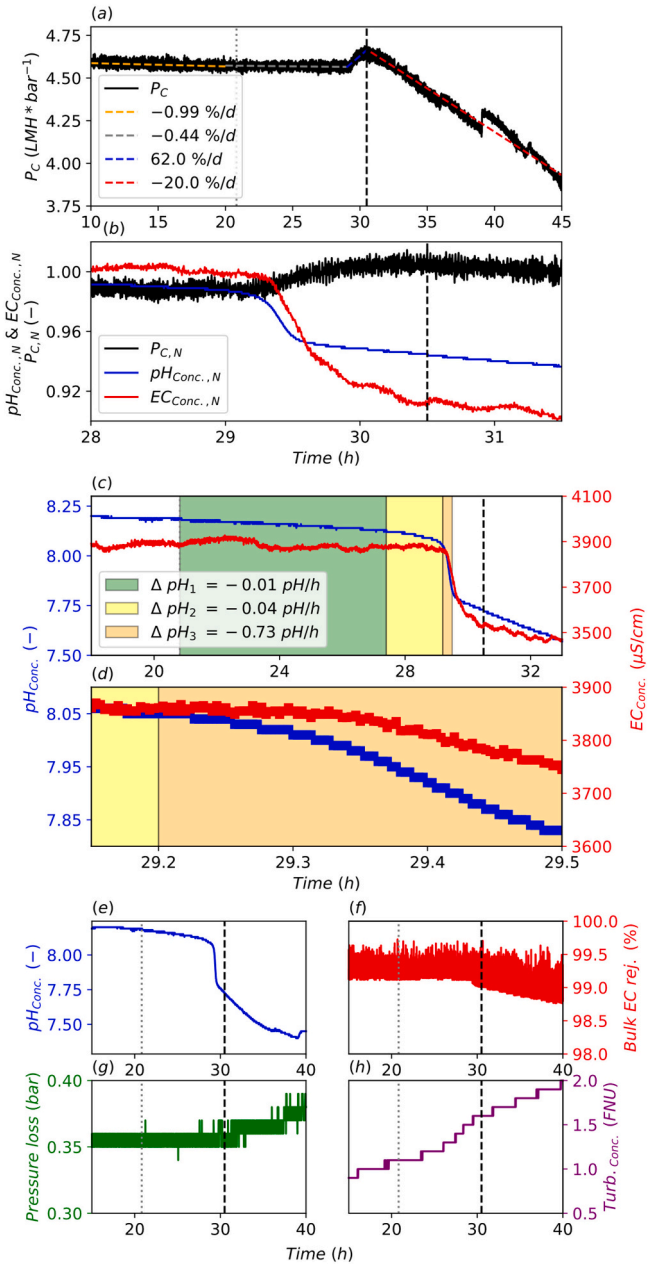

Fig. 2. Experiment 4″(1) operated at 20 LMH and 90 % recovery
a) Permeability curve with linear fits for decline b) Detailed view of scaling point for permeability, concentrate conductivity (EC) and pH; c) and d) Comparison of concentrate-EC and -pH; e) to f) comparison of different parameters for scaling detection; grey dotted and black dashed line represent the point in time of 0.03 pH drop and the temporal permeability maximum.

prior to the increase.

Three further temporary increases in permeability (after 36.4, 39.5 and 42.5 h) were detected. These permeability increases are discussed in detail in chapter 4.3. Another example of a permeability increase within a scaling event was observed in Experiment 4 (2), which is described in the Supplementary Information, chapter 2.1. Besides the clear signs for $CaCO_3$-scaling from online monitoring, i.e., drops in concentrate-pH, concentrate-EC, and permeability, the presence and analysis of precipitates in the concentrate samples also confirmed $CaCO_3$-precipitation; see chapter 2.5 of the Supplementary Information.

Fig. 2 c) and d) provide a more detailed view and comparison of concentrate-pH and -EC. Both parameters gave an earlier (approximately one hour) and more significant scaling sign than the permeability (the first permeability maximum is represented by the black dashed line). Moreover, the pH started to decline well in advance, whereas the EC fluctuated without a significant downward trend. The dropping pH accelerated over time and can be divided into three zones: low decrease (green) to high decrease (orange).

The pH started to decrease slightly about 10 h before the sharp drop in pH and EC. Moreover, the heavy drop of pH was about 5–10 min earlier than that of EC, see Fig. 2 d). In the study by Waly et al. [24], a drop of at least 0.03 pH units was defined as induction time, which would be reached after approximately 22 h, well before the permeability response (after about 30 h).

Fig. 2 e) to h) compare the concentrate-pH with other typical parameters for scaling detection (EC-rejection, hydraulic pressure loss and concentrate turbidity). The grey dotted line represents the induction time according to a drop of at least 0.03 units and the black dashed line the permeability maximum. Both retention and pressure loss showed the first signs of scaling later than the pH. On the other hand, the concentrate-turbidity showed an early increase (even before the pH; see chapter 2.2 of the Supplementary Information), which could indicate the formation of particles and, thus, incipient scaling. However, the turbidity signal increases constantly and does not show a strong bend, as is the case with the pH and EC values of the concentrate. Moreover, other experiments showed that false or no warnings were issued during the monitoring of turbidity in the case of scaling (Supplementary Information; chapter 2.2 Fig. S3 b). This is presumably explained by the nature of an optical measurement, which is prone to the accumulation of solids onto the measurement cell. In addition, treating real feedwaters is associated with high fluctuations of turbidity, e.g., for surface waters due to seasonal rainfall events [83]. Since feed turbidity fluctuations influence the concentrate turbidity measurement even more (due to the hydraulic concentration factor), the experience with false and missing warnings in the case of scaling and the more timely, reliable and often significant response of the concentrate-pH, the turbidity measurements were not further investigated in this study. However, concentrate turbidity might be considered an effective tool for early scaling detection for non-pH effective scalants, such as $CaSO_4$ [8]. Moreover, as later explained in chapter 4.3, the constant increase of turbidity in Fig. 2 h) might indicate incipient $CaCO_3$-crystals transported to the bulk and rinsed out. Another possible indicator of scaling might be the concentrate temperature, since the formation of $CaCO_3$ is an exothermic reaction. An example for temperature monitoring is included in chapter 2.3 of the supplementary Information.

Fig. 3 shows Experiment 2.5″(1) with a scaling event after around 31 h of operation. Coinciding with the experiments with the 4″ plant the earliest signs of $CaCO_3$-scaling is the concentrate-pH drop followed by the concentrate-EC (Fig. 3 b) significantly before the permeability drop. As with the 4″ plant (Fig. 2 a) the permeability dropped initially at a relatively low rate (linear fit yellow dashed line) and then reached a plateau (slight increase blue dashed line) for approximately two hours (Fig. 3 a). Then a heavy permeability decline was noticed (red dashed line). In contrast to the 4″ experiment no significant permeability increase was noticed, but a slight increase shortly before the heavy permeability drop (linear fit blue dashed line).

Fig. 3 c) depicts the concentrate-pH and -EC of Experiment 2.5″(1) over time. The pH started to drop approximately 10 h before the permeability drop. The grey dotted line represents the drop of 0.03 pH units as the induction time [24]. The induction time based on the concentrate-pH was thus reached approximately one hour before a heavy drop of concentrate-pH and -EC was noticed. Furthermore, bulk EC-rejection and pressure loss did not indicate scaling in advance (Fig. 3 d). The rejection started to drop concurringly with dropping concentrate-EC. Therefore, the concentrate-pH is also highly suitable for the early scaling detection in the 2.5″ plant. Moreover, additional data in Fig. S5 of the Supplementary Information show that pH-monitoring of concentrate samples in open-beaker tests could be a viable tool for the

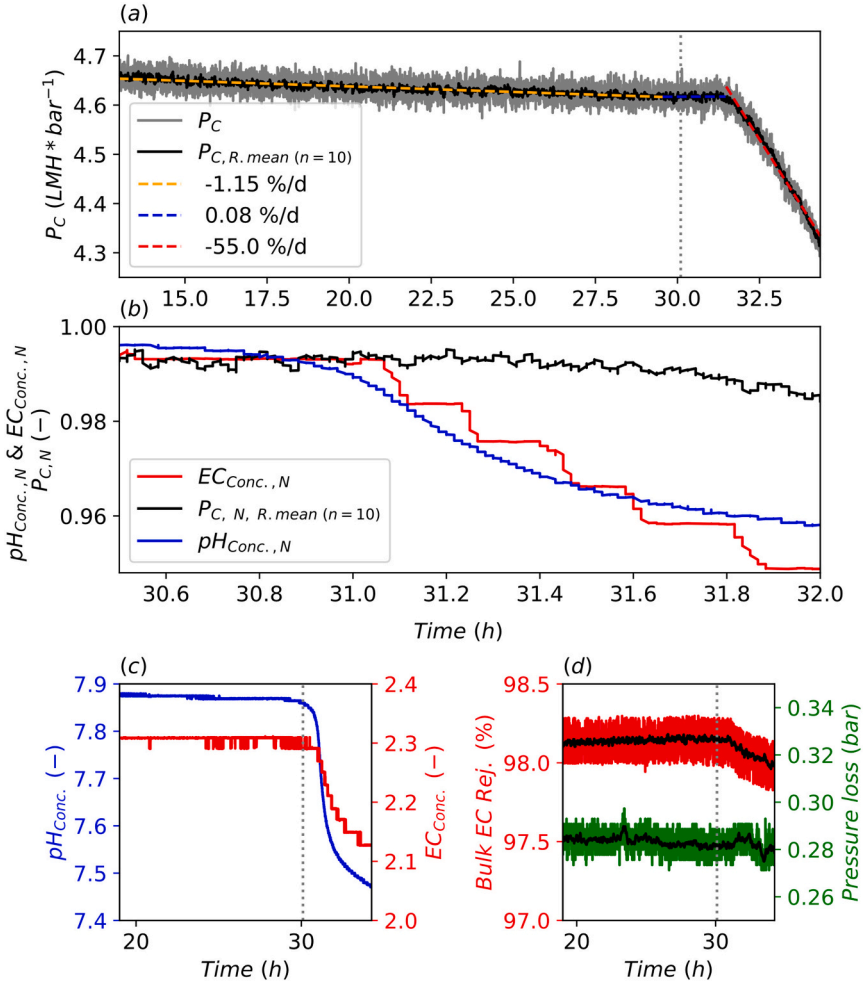

Fig. 3. Experiment 2.5″(1) Operated at 35 LMH and 85 % recovery:
a) Permeability over time, b) comparison of permeability and concentrate-pH and -EC over time c) detailed comparison of concentrate-pH and -EC, d) Rejection and pressure loss over time; grey dotted line represents the concentrate-pH drop by 0.03 units.

early $CaCO_3$-scaling detection, too.

Fig. 4 a) shows Experiment 2.5″(2), which was operated for over a month. A moderate and constant permeability decline was observed from the beginning on (linear fit blue dashed line with $R^2 = 0.97$). The decrease in permeability is unlikely to be due to $CaCO_3$-scaling, as the concentrate-pH showed no downward trend. Possible reasons could be colloidal fouling or biofouling, since, as it is typical for fouling, salt passage and pressure loss also increased over time (not shown) [84–86]. After 33.8 days of operation, the recovery was increased from 85 to 90 %, resulting in $CaCO_3$-scaling, as evidenced by a decrease in both permeability and concentrate-pH.

Fig. 4 b) zooms into Fig. 4 a) and depicts the scaling point after the recovery increase. Again, the concentrate-pH gave the earliest sign of $CaCO_3$-scaling. While the permeability dropped with the same slope as it did before for multiple hours, the pH decreased almost simultaneously with the increasing recovery. Without scaling, the pH increase due to the increasing concentration of HCO_3^- would have been comparable to that of the concentrate-EC (see Fig. S4 of the Supplementary Information). The EC loss due to $CaCO_3$ precipitation is overcompensated by the increasing EC due to the increasing recovery (see also Fig. S2 in the Supplementary Information). Since the solubility of $CaCO_3$ is relatively low [31], EC-response in a high strength concentrate is low for the precipitation of $CaCO_3$. Approximately seven hours after the first scaling sign, a forward flush was initiated. As expected for the low recovery (< 10 %), the concentrate-EC almost immediately reached the feed-EC.

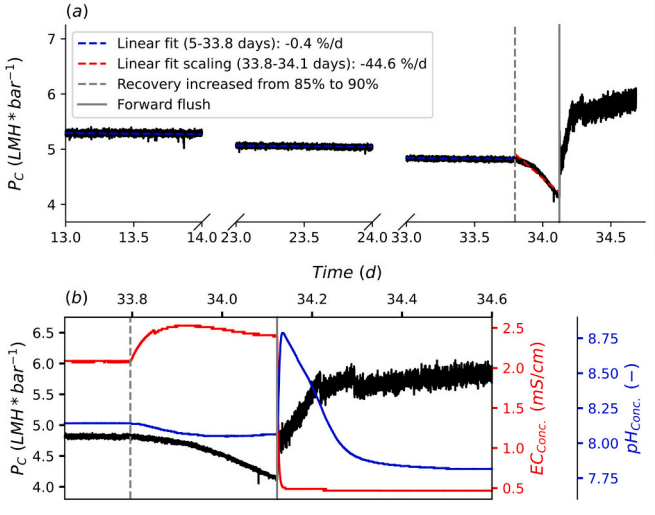

Fig. 4. Experiment 2.5″(2): a) Permeability curve over 34.5 days (broken axis) with linear fit for permeability decline b) Scaling point after recovery increase from 85 to 92 % (grey dashed line) and initiated forward flush (solid grey line); Operated until forward flush at 25 LMH.

However, the concentrate-pH increased drastically, and it took nearly seven hours until the pH approached the feed-pH (discharged brine was also measured with handheld pH device, which confirmed the increase). Although the washout of the CP layer might partly explain the pH increase, this would not explain the long duration of the pH peak. Therefore, it is likely that $CaCO_3$ is dissolving to Ca^{2+} and HCO_3^-, connected to a pH increase, by reversing Eq. (2). This would also explain the relatively high increase of permeability, which is for once due to the dissolution of the CP layer (lowering the osmotic pressure at the membrane), but presumably $CaCO_3$-nuclei that have formed are also sheared off the membrane and then dissolved due to the high concentration gradient caused by flushing with feedwater. The same pH increase after a scaling event with subsequent flushing was demonstrated in experiment 2.5″(3), see Supplementary Information Fig. S6.

This is an indication that the inherent flushing in discontinuous operation could prevent scaling, firstly by lowering the concentration and increasing the driving force of dissolution of crystals, and secondly by removing incipient deposits from the membrane through a higher crossflow. It is therefore claimed that the concentrate-pH is a powerful and robust tool, not only, as shown, for continuous operation, but in particular for discontinuous processes, such as batch- and semi-batch operation (e.g. closed-circuit RO). Firstly, to detect early $CaCO_3$-scaling under transient conditions at an early stage, and secondly, to control the inherent flushing of discontinuous processes. For instance, in closed-circuit RO operation, concentrate-pH could be used to discriminate a critical duration of a closed-circuit interval indicative of incipient scaling before concentrate-EC, permeability, pressure loss, or retention respond. Finally, in the case that in a flushing mode $CaCO_3$ is dissolving, the concentrate-pH could be used to determine the flushing time until dissolution is finished, i.e., feed and concentrate-pH roughly match.

4.2. Scaling mitigation by early detection

The experience gathered in early detection was applied to mitigate scaling by timely intervention: in the event of a continuously decreasing concentrate-pH, a forward flush was triggered (temporarily lowering recovery and flux significantly). To reduce the effect of overlapping fouling as experienced in Experiment 2.5″(2), the flux was lowered to 20 LMH. In the first step, the limiting recovery for the BW30 membrane was determined to be 82.5 % ($SI_{Calcite} = 1.95–2.0$) by conducting Experiment 2.5″(4): Quickly after reaching the maximum concentrate-EC (approximately 2.35 mS/cm), $CaCO_3$-precipitation was evident, indicated by the dropping concentrate-pH. Again, concentrate-pH indicated scaling significantly earlier than decreasing permeability, concentrate-EC or rejection. The results can be found in chapter 2.6 of the Supplementary Information.

Fig. 5 a) shows the permeability curve of the longtime (> 65 days) scaling Experiment 2.5″(5), in which the concentrate-pH was used to trigger forward flushing. The experiment was operated at varying recoveries (75 to 82.5 %) and constant flux (20 LMH). The critical recovery (82.5 %) was in total ten times applied. Fig. 5 b) to e) give examples of the applied $CaCO_3$-scaling prevention by forward flushing initiated by the concentrate-pH. The observed constant small permeability loss (linear trend blue dashed line) is, as in Experiment 2.5″(2), presumably related to fouling and not to $CaCO_3$-scaling. However, due to the lowered flux (from 25 to 20 LMH), the permeability loss in Experiment 2.5″(5) is almost three times lower. Moreover, in contrast to Experiment 2.5″(2), no increase in pressure loss or salt passage over time was noticed.

In Fig. 5 c), the recovery after forward flushing was set to 80 %, which, in contrast to previous and subsequent adjustments, resulted in strong signs of precipitation, indicated by a drop in the concentrate-pH. However, the performed forward flush prevented significant permeability loss.

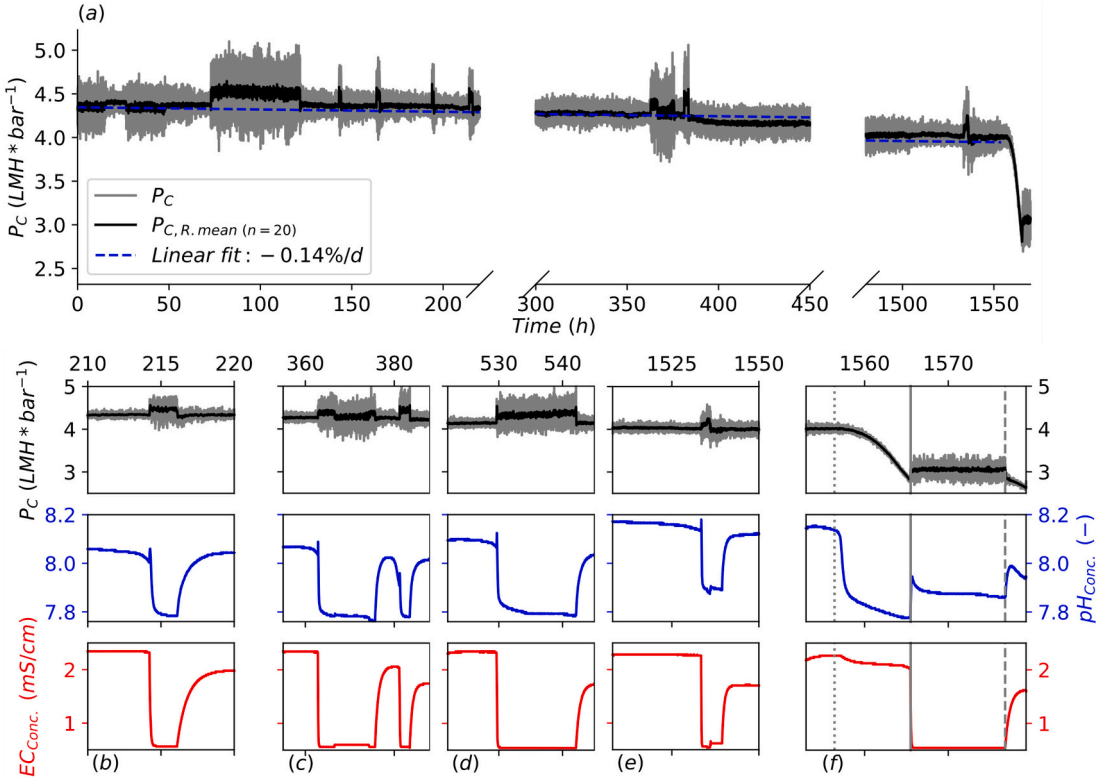

Fig. 5. Experiment 2.5″(5): Long time operation with concentrate-pH triggered forward flushing operated at 20 LMH and recoveries of 75 to 82.5 %: a) Permeability over time; b) to e) examples of scaling mitigation after reaching the critical recovery (82.5 %); f) Scaling point with delayed forward flush. Grey dotted line: concentrate drop by 0.03 pH-units; solid line initiated forward flush and dashed line increase of recovery to 75 %.

Calculating the induction times by applying the drop of 0.03 pH units [24], the average induction time for the runs shown in Fig. 5 b) to d) was 10.3 h. The general decreasing trend from 13 to 7.5 h from b) to d), respectively, might indicate that despite the forward flushes some crystals attach to the membrane, which lower the induction time acting as a seeding. Moreover, the temperature rose over the whole experiment by approximately 2 K, which reduces the solubility of $CaCO_3$.

To assess whether some crystals deposited onto the membrane would develop into membrane scaling with longer induction times, the process was continued for >1100 h (from approximately 400 to 1500 h) at a recovery of 75 % ($SI_{Calcite}$ = 1.71). However, there were no signs of scaling. On the contrary, the overall permeability decreased to a lesser extent, i.e., after 1000 h the measured permeability curve was no longer below, but above the linear fouling trend (Fig. 5 a). The recovery was then again increased to the critical recovery (Fig. 5 e), and the same early signs of precipitation were detected, which triggered a forward flush.

Interestingly, although the saturation index slightly increased ($SI_{Calcite}$ = 1.98) due to the higher temperature, the induction time increased to 24 h, which is more than double the previous average. One possible explanation could be a fouling layer that interacts with the membrane surface. Steiner et al. [29] suggested that negatively charged membrane surfaces, e.g., due to negatively charged carboxyl groups, attract calcium ions, acting as nucleation-sites. The accumulation of a fouling layer could thus occupy or lower the accessibility of negatively charged carboxyl groups for calcium ions, reducing the proneness to $CaCO_3$-scaling. In contrast, Thompson et al. [87] found that $CaSO_4$-scaling in the presence of a previously developed biofilm had a greater surface coverage and crystal number than $CaSO_4$-scaling in the absence of a biofilm. This effect could be investigated in further studies, e.g., by measuring the zeta-potential before and after the formation of a fouling layer.

Finally, the recovery was again increased to 82.5 %, but this time without immediate intervention by forward flush to investigate the scaling scenario. Fig. 5 f) shows the resulting scaling point of this experiment. The grey dotted line represents the point of induction time when the pH dropped by 0.03 units. The permeability started approximately four hours later to decrease significantly. Ten hours after reaching the induction time and a permeability loss of around 30 %, a forward flush was initiated (grey solid line) for several hours. However, the forward flush did not show a significant improvement in the permeability which only increased due to the lowered CP. Interestingly, after stopping the forward flush and setting a recovery of 75 % (grey dashed line) heavy scaling signs were present, i.e., decreasing pH and permeability, although previously, no signs of scaling were found for the same conditions over extended periods (> 1100 h). Therefore, it is likely that the membrane was partially covered with scale, which was not removed by the forward flush, and led to secondary nucleation and thus drastically lowered the necessary saturation and induction time.

In each time when the critical recovery was applied a clear induction time was noticed. This means that, after the recovery was increased and the system reached a steady-state, all relevant parameters (permeability, salt-retention, concentrate-pH and -EC) were constant for a certain period (between 7.5 and 24 h before the pH dropped by 0.03 units). Forward flushing presumably resets the induction time, as reported for flow reversal [50–52], too, allowing to operate the plant repeatedly at the edge to scaling. This is in contrast to the observations of Mitrouli et al. [23], who did not detect an induction time for $CaCO_3$-scaling. On the other hand, an undetected induction time could be related to a high supersaturation state if a steady state is not reached before precipitation, as seen in Experiment 4″(2) in Fig. S2 (Supplementary Information).

Moreover, it is astonishing that relatively high saturations, e.g., at a recovery of 75 % with a $SI_{Calcite}$ = 1.71 can be reached without signs of $CaCO_3$-scaling over >45 days. This is in particular interesting, since the plants were operated with constant concentrate recirculation and discharge (feed and bleed), which leads to much higher hydraulic retention times of the concentrate, see Table S5 (Supplementary Information). Compared to conventional designs where high recoveries are achieved by implementing multiple stages, the hydraulic retention time of the concentrate was in the experiments up to 30 times higher. Therefore, the experiments represent a worst-case scenario in terms of scaling, and yet, no scaling was experienced at high supersaturation without dosing antiscalants. One possible explanation could be the relatively high feed DOC (2–4 mg C/L, see chapter 1.1 of the Supplementary Information). Components of the DOC, e.g., humic substances may act as a natural antiscalant and increase the induction time [88,89] by blocking active crystal growth sites [90]. For the given feed water, a presence of humic substances is expected (Supplementary Information chapter 1.1).

4.3. Model development and simulation of experimental data

From the presented results, various questions arise, e.g., why does the concentrate-pH react earlier than other parameters? Why does the permeability react considerably later (Fig. 3) than pH and EC, and in some cases, even increases before it starts to drop (permeability bumps in Fig. 2 and Fig. S2), although precipitation within the bulk is evident? In the following, these open questions are addressed by various water chemistry models, simulations and estimations of the concentrations directly at the membrane using the concentrate composition of Experiment 4″(1) (see detailed description in chapter 3 of the Supplementary Information).

As discussed before, the solubility of $CaCO_3$ is relatively low [31], explaining the initially relatively low response of the EC. However, when looking at Experiment 4″(1), it is remarkable that the concentrate-pH dropped by 0.15 units within eight hours and at the same time no significant downward trend but mainly fluctuation of the concentrate-EC was noticed. Considering that the formation of 1 mol of $CaCO_3$ leads to the consumption of 1 mol of Ca^{2+} and 2 mol of HCO_3^-, see Eq. (2), and that Ca^{2+} and HCO_3^- induce an equivalent conductivity of 53.7 and 36.5 µS/cm * (meq/L) $^{-1}$, respectively [33], the late concentrate-EC response is surprising. To investigate possible reasons, three simulations based on a developed PhreeqC model were conducted.

At first, the influence of the concentrate-pH on the distribution of species and the concentrate-EC was investigated in Simulation 1. Fig. 6 depicts the influence of the pH on the distribution of selected calcium and TIC species. It shows that the EC has a maximum at approximately pH 7.6, and then starts to decline with an increasing pH, although the solution composition is, besides the varied pH, constant. The progression of the EC follows in a good approximation, the HCO_3^- curve. The HCO_3^- concentration decreases at lower pH (lower 7.7) due to an increasing fraction of dissolved CO_2, while at higher pH, the concentration reduces primarily due to the formation of aqueous complexes ($CaCO_{3,aq}$) and partly due to shifting of the TIC to CO_3^{2-}. For Ca^{2+} a steady decline with increasing pH is observed, predominantly explained

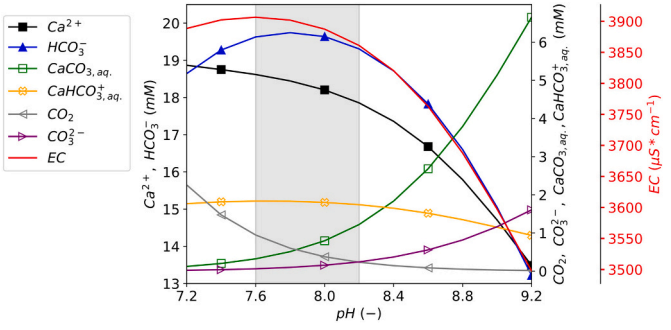

Fig. 6. Simulation 1: Influence of pH on the distribution of species and the conductivity of the concentrate 4″(1). The grey box represents the drop of pH in the scaling event of 4″(1).

by the increase of the aqueous complex $CaCO_{3,aq}$. Therefore, the concentration of Ca^{2+} and HCO_3^- decreases at higher pH mainly due to the formation of aqueous complexes, and since (uncharged) complexes do not contribute [91] or contribute less to the EC (charged complexes), the concentrate-EC decreases with increasing pH at otherwise same conditions. The grey transparent box of Fig. 6 shows the area in which the concentrate-pH of Experiment 4″(1) dropped from 8.2 to 7.6, which yields, according to Simulation 1 (only pH is varied), to a conductivity increase of roughly 50 µS/cm, primarily explained by less aqueous complexes at lower pH-values. It should be noted that, within the concentrate of Experiment 4″(1), many more aqueous complexes are present, e.g., $CaSO_{4,aq}$, $MgSO_{4,aq}$ and $NaSO_{4,aq}^-$. Fig. 6, however, only depicts the complexes which are highly influenced by the pH.

In Simulation 2, the amount of CO_2 was determined to lower the pH from 8.2 to 7.6 as observed in Experiment 4″(1), see Fig. 2. Fig. 7 shows that roughly 2 mM of CO_2 is necessary to reach a pH of 7.6. Moreover, it reveals that the majority of CO_2 will react to HCO_3^- due to the high buffer capacity of the concentrate.

The reasons for the initial low to no concentrate-EC response in the scaling event of Experiment 4″(1) can thus be summarized as follows: The released CO_2 reacts mainly in the well-buffered concentrate to form HCO_3^- (Fig. 7) and thus partially compensates for conductivity lost through precipitation. On the other hand, as the concentrate-pH decreases, e.g., from 8.2 to 8.05 (grey area of Fig. 6), the number of aqueous complexes decreases, resulting in an increase in Ca^{2+} and HCO_3^- (further results in chapter 3.1 of the Supplementary Information), which partly offsets the lower EC value caused by precipitation. This confirms the experimental data where the pH gave earlier and more significant signs of precipitation than EC.

In Simulation 2, the solution is only adjusted by adding CO_2 and does not consider that the concentrations of Ca^{2+} and HCO_3^- decrease. Therefore, Simulation 2 will slightly overestimate the amount of CO_2 since it does not consider a decrease of buffer capacity due to precipitation of HCO_3^-. Simulation 3 was performed to analyze the changing solution composition for seven selected points in time from no-scaling (pH = 8.2) to heavy scaling conditions (pH = 7.6) of Experiment 4″(1). The simulation provides the solution composition (e.g. EC, calcium and TIC concentration) for the respective pH values and predicts that a total of 1.83 mM of $CaCO_3$ will be precipitated to lower the pH from 8.2 to 7.6. It also supports the results of Simulation 2 by showing that the TIC is not reduced by a factor of two of the molar release of $CaCO_3$, according to Eq. (2), but is approximately equimolar to the precipitated $CaCO_3$, since the released CO_2 mainly forms HCO_3^- (Table S9 Supplementary Information).

Fig. 8 a) compares the simulated progression of concentrate-EC and $SI_{Calcite}$ (Simulation 3) with the measured concentrate-pH and EC. The simulation forecasts that the concentrate-EC will only drop by 22 µS/cm, representing a decrease of roughly 0.5 %, when the pH drops by 0.15 units (from 8.2 to 8.05). At the same time, the measured concentrate-EC fluctuates with a slight decreasing trend (3884 µS/cm ±14 µS/cm), with a maximum fluctuation range of 77 µS/cm. Therefore, in contrast to the concentrate-pH drop of 0.15 units, the concentrate-EC change due to incipient precipitation cannot be distinguished from fluctuations.

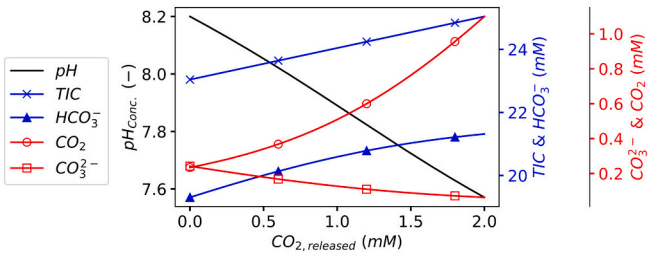

Fig. 7. Simulation 2: Influence of released CO_2 on pH and inorganic carbon species in the bulk concentrate of 4″(1).

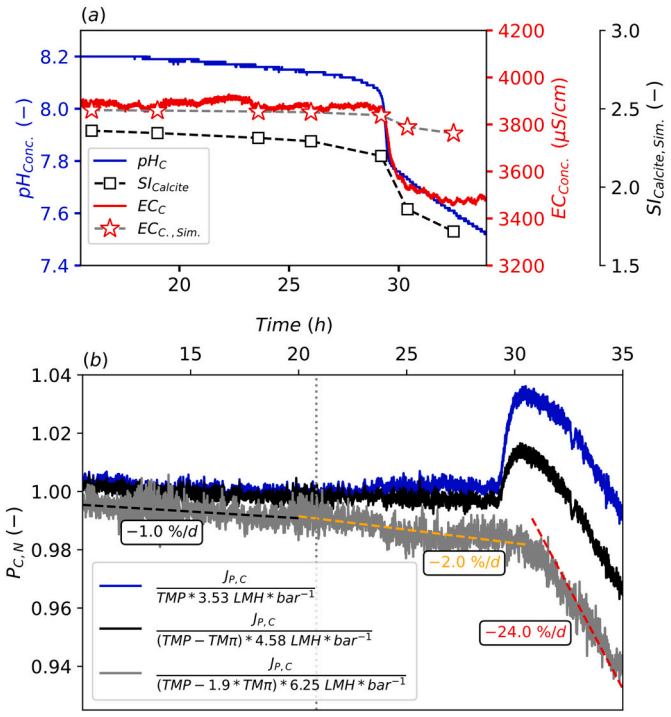

Fig. 8. a) Simulation 3: Comparison of measured and simulated concentrate-EC and simulated $SI_{Calcite}$ for seven points (dashed lines are not simulated and are included solely for better orientation); b) Normalized and corrected permeabilities: temperature (blue), temperature and osmotic pressure in the bulk (black) and at the membrane with β = 1.9 (grey). All measured permeabilities are rolling means (n = 5); Dashed lines give the linear fit for the permeability decline and grey dotted line represents the drop of 0.03 pH units.

Interestingly, if only the induced conductivity of ions is taken into account, the EC-drop would greatly overestimate the conductivity loss from 8.2 to 8.05 at about 80 µS/cm (see chapter 3.2 of the Supplementary Information). This showcases the previously revealed influence of the aqueous complexes, and that the released CO_2 will partially react to form HCO_3^- and thus solely applying Eq. (2) will not reflect on the experimental data.

After an excellent fit of the first five simulated concentrate-EC values, the simulation predicts a much lower EC-decrease than measured. Since the simulation is based on the concentrate-pH, one possible explanation for the deviation is the precipitation of sparingly soluble salts that do not affect the pH, in addition to the $CaCO_3$-precipitation. However, other supersaturated salts in the concentrate are pH-affective salts, e.g., dolomite, but due to their concentration and the measured pH-response, they are probably not relevant for the strong decrease in the concentrate-EC. Gypsum ($CaSO_4{:}2H_2O$), on the other hand, is slightly undersaturated in the bulk and likely supersaturated within the CP-layer and its precipitation will not (significantly) affect the solution pH. Considering a CP-factor β = 1.9 (the selection of the value is justified later), $CaSO_4$ will be supersaturated. Moreover, formed $CaCO_3$-particles could act as surface for heterogenous nucleation within the CP layer.

Zarga et al. [92] investigated the co-precipitation of $CaCO_3$ and $CaSO_4$ and found that, with a calcium to sulfate surplus (molar ratio of calcium to sulfate of roughly 1.7), $CaCO_3$ nucleates first, indicated by pH, alkalinity and slight Ca^{2+} drop followed by gypsum precipitation without affecting pH and alkalinity, but with a significant drop of the calcium concentration [92]. This corresponds to the experiments of the present study with a high calcium surplus (molar ratio of 3.7) and a first relatively low EC drop explained by $CaCO_3$-precipitation.

The later measured high EC drop, which is not predicted by the simulations, see Fig. 8 a), could thus be connected to $CaSO_4$

precipitation. Since the solubility of $CaSO_4$ is much higher than that of $CaCO_3$ [92], its precipitation would yield in a much more pronounced EC response. In addition, the analyzed precipitates from concentrate samples of Experiment 2.5″(2), taken before scaling occurred, showed, in addition to oxygen (~74 %) and calcium (~25 %) also sulfur (~0.5 %) as significant element in the sum spectrum (all other elements below 0.17 %). This indicates a possible precipitation of $CaSO_4$ in addition to $CaCO_3$ (see chapter 2.4 of the Supplementary Information). Unfortunately, no samples of the concentrate were collected during the scaling event for further analysis. Therefore, this should be investigated in further studies by means of membrane autopsies of scaled membranes to identify other precipitated salts. However, chemical cleaning of scaled membranes typically showed best permeability recovery by applying acids suggesting mainly $CaCO_3$ precipitates on the membrane (see Supplementary Information chapter 2.7). Further results of Simulation 3 are summarized in chapter 3.2 of the Supplementary Information.

However, one question remains: why, despite clear signs of bulk crystallization, is a certain lag time experienced before distinct indications of membrane scaling occur? For instance, the simulated $SI_{Calcite}$ in Fig. 8 a) dropped within 15 h by 0.16 units representing almost 60 mg/L of precipitated $CaCO_3$ while neither an accelerating permeability decrease nor an increasing pressure loss nor a decreasing retention (e.g., Fig. 2) were experienced during the same period. On the contrary, within the same time (approximately 15 to 30 h of operation), the permeability initially began to decrease less and then increased drastically (grey and blue dashed line in Fig. 2 a), while the signs of bulk precipitation (decrease in concentrate-EC and -pH) intensified (Fig. 2 b). Furthermore, to the best of our knowledge, a permeability increase, i.e., permeability bump, (as presented in Fig. 2 and in Fig. S2 in the Supplementary information) or a delayed permeability response (Fig. 3) has not been discussed in the scientific literature so far, although the same phenomena can be seen in figures of other $CaCO_3$-scaling studies [25]. For example, in Fig. 2 of the study of Tzotzi et al. [25] a moderate drop in permeability is followed by an increase (first permeability bump), a heavy decrease and a further increase (second permeability bump), which was also seen in the present investigations. However, possible reasons for the increase are not discussed by the authors [25]. One possible explanation of the bump could be an increase in the net transmembrane pressure (see Eq. (5)) due to the lowered osmotic pressure in the cause of precipitation. This temporary increase could initially mask the decreasing permeability due to the first deposits of $CaCO_3$ on the membrane.

To prove this hypothesis in the present study, the permeabilities are not only corrected by the osmotic pressure, as shown in Eq. (3) to (5), but additionally by assuming a CP layer using Eq. (6). As depicted in Fig. 8 b), the bump is significantly more pronounced without correction of bulk osmotic pressure (blue curve), though a clear bump is visible also with correction based on the concentrate-EC (black curve). However, a CP layer results in higher concentration at the membrane compared to the bulk. Therefore, measured changes of the bulk, and thus the applied correction functions, will underestimate the change directly at the membrane, e.g., the effect of precipitation on the driving force. Thus, a CP factor of $\beta = 1.9$ was assumed to further correct the permeability which smoothened the bump (grey curve). The fitted β value agrees well with the expected range reported in the literature, for example as observed for the Reynolds number in laminar flow [93], as well as for calcium and relevant aqueous complexes [94]. Moreover, it only deviates by about 1.5 % from the permeability calculated from the membrane supplier data sheet at standard conditions with neglectable CP (see calculations in the Supplementary Information chapter 2.8).

Considering CP in the permeability calculation further on reveals that imminent signs of bulk precipitation reflect also on amplifying permeability loss. Fig. 8 b) shows that approximately 10 h before the heavy permeability drop, the decrease in permeability has already doubled (black vs orange dashed line as linear fit). Roughly simultaneously the concentrate-pH reached the induction time based on a drop of 0.03 units (grey dotted line).

Without considering CP, this trend is not visible (black and blue line) and indicates an increase rather than a decrease in permeability. Moreover, Fig. 2 a) shows that the decrease in permeability initially flattens, stabilizes and then increases shortly before and within a scaling event (yellow, grey and blue dashed line), when CP is not considered. Therefore, CP effects mask initially the loss of permeability caused by deposits on the membrane.

Moreover, it is likely that permeability loss due to initial scale deposits is reversible. Formed deposits can dissolve again, as in the case of the timely intervention where a significant and sustained increase in the concentrate-pH was observed when a forward flush was performed (see Fig. 4 b). This is likely attributed to the initial formation of deposits consisting of relatively small particles on the membrane surface. Onuma et al. [95] found that within the first few hours of precipitation, nanodots (5–10 nm) dock onto surfaces before larger particles (20–30 nm) cover the surface. Moreover, in incipient scaling, functional groups are potentially covered first, e.g., negatively charged carboxylate groups with positively charged calcium ions [30]. Therefore, forward flushing can dissolve small crystals, shear them off the membrane or trigger back-diffusion into the bulk, resulting in stable permeability over long operating period. This can be seen in Fig. 5, when forward flushing is applied in time. In addition, formed nuclei might initially only partly cover the membrane and are presumably partially transported to the bulk by diffusion and then to a certain extent discharged with the brine or may dissolve when concentrate is mixed with fresh feed.

After a certain lag time, a heavy permeability drop is experienced, which is typically not recoverable, as seen in Experiment 2.5″(5) when the forward flush was conducted 10 h after reaching the induction time (Fig. 5 f). Elevated time increases the likelihood of larger [95] and more particles, which cover more surface and can attach not only to charged surfaces but directly to the membrane polymer. Moreover, they act as further nucleation sites for other deposits (e.g., $CaSO_4$) and for secondary nucleation, which can trigger a chain reaction, explaining the severe permeability drop and the inefficiency of forward flushing. The assumption of a certain lag time until irreversible scaling occurs could also explain the difference between the results of the 4″ and 2.5″ systems. Although the same feedwater was used, the limiting recovery of the 4″ plant was in general higher than of the 2.5″ plant, despite the 2.5″ plant was operated at higher cross flow velocity (see chapter 3.1). If the system volume is related to the installed membrane-surface ($m^3_{Volumen}/m^2_{Membrane}$) the ratio of volume to membrane area is six times greater for the 2.5″ plant, which results in a significantly higher hydraulic retention time (HRT) of the concentrate (see Table S5 Supplementary Information). Flushing out formed incipient nuclei is much more likely at low HRTs, and thus in the 4″ plant, which might explain the longer lag time. This could also explain the constant increase in turbidity in the brine pipe (Fig. 2 h) which indicates an increasing concentration of washed-out particles.

Since the feed and bleed operation with concentrate recirculation chosen in the present study is rather atypical for industrial applications, it can be assumed that the identification of incipient scaling could be further facilitated in a conventional RO multi-stage operation with a significantly lower HRT of the concentrate.

5. Conclusion

This study demonstrates the effectiveness of early $CaCO_3$-scaling detection by pH measurement using pilot- and laboratory-scale plants with spiral-wound RO membranes and a real water matrix.

A decrease in bulk concentrate-pH correlates reliably with $CaCO_3$-scaling, earlier and more accurately than other parameters such as conductivity (EC), turbidity, permeability, salt retention, and hydraulic pressure drop. The delayed and less pronounced response of concentrate-EC is attributed to buffering effects and complex dissociation, as revealed by water chemistry models. On the other hand, the

delayed permeability response can be assigned to concentration polarization effects, which also explain the observed temporary permeability increase during scaling events.

Incipient $CaCO_3$-scaling is reversible. Therefore, timely intervention with forward flushing effectively counteracts the onset of $CaCO_3$-scaling, as demonstrated in long-time experiments. Utilizing pH-triggered forward flushing enabled stable operation for >65 days at high recoveries ($SI_{Calcite}$ up to 2.0) without antiscalants.

Monitoring the concentrate-pH is thus a practical tool for $CaCO_3$-scaling mitigation, optimizing or even obviating antiscalant dosing, and determining critical recoveries for RO and NF systems prone to $CaCO_3$-scaling.

These findings suggest high applicability of the proposed method for early scaling detection for discontinuous operation such as semi-batch or batch RO warranting further investigation.

CRediT authorship contribution statement

Martin Futterlieb: Conceptualization, Methodology, Validation, Formal analysis, Investigation, Data curation, Writing – original draft, Writing – review & editing, Visualization, Supervision. **Stefan Panglisch:** Conceptualization, Validation, Resources, Writing – review & editing, Supervision, Project administration, Funding acquisition.

Declaration of Generative AI and AI-assisted technologies in the writing process

The authors' original prepared draft was partly edited using Grammarly Premium and Perplexity-Pro to enhance grammar, expression, and readability. In addition, Perplexity Pro assisted in debugging Python code used for data processing. After using these tools, the authors reviewed and edited the content as needed and take full responsibility for the content of the publication.

Declaration of competing interest

The authors declare that they have no known competing financial interests or personal relationships that could have appeared to influence the work reported in this paper.

Acknowledgments

This research was partly conducted in the framework of the project KonTriSol (https://kontrisol.de/) and MAMDIWAS. The project KonTriSol was funded (grant no. 02WAV1530C) by the Federal Ministry of Education and Research of Germany (BMBF) and co-financed by the German Technical and Scientific Association for Gas and Water (DVGW). The project MAMDIWAS is funded (grant no. 02WAS1719A) by the BMBF. The 2.5" plant was partially funded within the framework of "Innovative Wassertechnologie im FutureWaterCampus (InnoWat) by the European Regional Development Fund (ERDF) - EFRE-NRW 2014-2020 Program. The authors would like to thank Endress+Hauser GmbH+Co KG for their cooperation and the supply of measuring equipment for the 4" plant. Moreover, we are thankful for the membrane supply from DuPont, Suez and Veolia. Furthermore, the authors are grateful for the lab assistance from Lucas Landwehrkamp and the SEM-EDX analysis from Silke Rink (Institut für Technologien der Metalle (ITM), University of Duisburg-Essen). The authors acknowledge the experimental contributions of Siddharth Shrikant Modak, Puneet Naresh Manghnani and Omar Ben Chobba in the context of their graduation theses at the University of Duisburg-Essen.

Appendix A. Supplementary data

Supplementary data to this article can be found online at https://doi.org/10.1016/j.desal.2025.119023.

Data availability

Data will be made available on request.

References

[1] B. Cyna, G. Chagneau, G. Bablon, N. Tanghe, Two years of nanofiltration at the Mery-Sur-Oise plant, France, Desalination 147 (2002) 69–75, https://doi.org/10.1016/S0011-9164(02)00578-7.
[2] M. Ophorst, J.d. Grooth, S.G.J. Heijman, E.M.H. Vaudevire, M. Jafari, Operation and performance analysis of direct hollow fiber nanofiltration: a pilot study at IJsselmeer, Sep. Purif. Technol. 349 (2024) 127786, https://doi.org/10.1016/j.seppur.2024.127786.
[3] M. Tuczinski, D. Stetter, S. Egner, Status quo: verfahrenstechnische Optionen; Abschlussbericht Arbeitspaket 1; Projektergebnisse des BMBF-Verbundprojekts KonTriSol, IWW Rheinisch-Westfälisches Institut für Wasserforschung gemeinnützige GmbH, TZW: DVGW-Technologiezentrum Wasser, Funding Code: 02WAV1530A, 2021, pp. 41.
[4] B. Mattheß, U. Müller, Nitratentfernung mit Umkehrosmose vom Konzept zur Umsetzung, DVGW energie | wasser-praxis (2023) 20–24.
[5] M. Sousi G. Liu S.G. Salinas-Rodriguez L. Chen J. Dusseldorp P. Wessels J.C. Schippers M.D. Kennedy van der W. Meer Multi-parametric assessment of biological stability of drinking water produced from groundwater: reverse osmosis vs. conventional treatment Water Res. 186 2020 116317 https://doi.org/10.1016/j.watres.2020.116317.
[6] OCWD. Purification process. 2023 15th of May 2023]; Available from: https://www.ocwd.com/gwrs/the-process/.
[7] R.S. Trussell, A.N. Pisarenko, Process benefits of ozone/BAC as pretreatment to membrane-based advanced treatment for direct potable reuse, Water Reuse 14 (2024) 146–159, https://doi.org/10.2166/wrd.2024.113.
[8] A.M. Schwiebert, J.A. Bush, A. Bray, I. Reyes, A. Cortijo, H. Portilla, P. García-Chevesich, C. Bellona, T.Y. Cath, J. Vanneste, Turbidity-based scaling detection system for batch reverse osmosis combined with gypsum crystal recovery, Desalination 586 (2024) 117817, https://doi.org/10.1016/j.desal.2024.117817.
[9] E.W. Tow, Q.J. Wei, A.R. Abraham, K.L. Chua, M.J. Plumley, J.H. Lienhard, Piloting batch reverse osmosis with a flexible bladder for water recovery from scaling-prone brine, Npj Clean Water 8 (2025) 30, https://doi.org/10.1038/s41545-025-00462-6.
[10] Panglisch, S. Membranverfahren - Grundlagen und Praxisanwendung, in: Wasseraufbereitung - Grundlagen und Verfahren DVGW Lehr- und Handbuch Wasserversorgung Bd. 6. Jekel, Martin; Czekalla, Chritoph. München, 2017.
[11] J. Benecke, J. Rozova, M. Ernst, Anti-scale effects of select organic macromolecules on gypsum bulk and surface crystallization during reverse osmosis desalination, Sep. Purif. Technol. 198 (2018) 68–78, https://doi.org/10.1016/j.seppur.2016.11.068.
[12] A. Rahardianto, B.C. McCool, Y. Cohen, Reverse osmosis desalting of inland brackish water of high gypsum scaling propensity: kinetics and mitigation of Membrane mineral scaling, Environ. Sci. Technol. 42 (2008) 4292–4297, https://doi.org/10.1021/es702463a.
[13] N. Konradt, J.G. Kuhlen, H.P. Rohns, B. Schmitt, U. Fischer, T. Binder, V. Schumacher, C. Wagner, S. Kamphausen, U. Muller, F. Sacher, P. Janknecht, R. Hobby, I.M.A. ElSherbiny, S. Panglisch, Removal of trace organic contaminants by parallel operation of reverse osmosis and granular activated carbon for drinking water treatment, Membranes (Basel) 11 (1) (2021) 33, https://doi.org/10.3390/membranes11010033.
[14] P. Riedinger, M. Brugger, Moderne Umkehrosmoseanlage mit Retentataufbereitung, Fachz. Bbr - Leitungsbau Brunnenbau Geotherm. (2018) 84–89.
[15] Stauder, S., Müller, U., Egner, S., Riedinger, P. PFAS-Entfernung mit Umkehrosmose und Aktivkohle. Energ. Wasser-Prax., 09/2024 (2024).
[16] J. Wang, C. Liu, S. Ding, Y. Yang, Nanofiltration (NF) application in drinking water treatment plants and the challenges of its concentrate management in China, Desalination 611 (2025) 118937, https://doi.org/10.1016/j.desal.2025.118937.
[17] T. Jain, E. Sanchez, E. Owens-Bennett, R. Trussell, S. Walker, H. Liu, Impacts of antiscalants on the formation of calcium solids: implication on scaling potential of desalination concentrate, Environ. Sci.: Water Res. Technol. 5 (2019) 1285–1294, https://doi.org/10.1039/C9EW00351G.
[18] L.F. Greenlee, D.F. Lawler, B.D. Freeman, B. Marrot, P. Moulin, Reverse osmosis desalination: water sources, technology, and today's challenges, Water Res. 43 (2009) 2317–2348, https://doi.org/10.1016/j.watres.2009.03.010.
[19] M. Feiner, S. Beggel, N. Jaeger, J. Geist, Increased RO concentrate toxicity following application of antiscalants - acute toxicity tests with the amphipods Gammarus pulex and Gammarus roeseli, Environ. Pollut. 197 (2015) 309–312, https://doi.org/10.1016/j.envpol.2014.11.021.
[20] M.N. Mangal, S.G. Salinas-Rodriguez, J. Dusseldorp, A.J.B. Kemperman, J. C. Schippers, M.D. Kennedy, W.G.J. van der Meer, Effectiveness of antiscalants in preventing calcium phosphate scaling in reverse osmosis applications, J. Membr. Sci. 623 (2021) 119090, https://doi.org/10.1016/j.memsci.2021.119090.
[21] D. Chowdhury, A. Kuras, T. Cath, A.S. Hering, A. Melin, T.Y. Cath, K. Villez, Autonomous online optimization of a closed-circuit reverse osmosis system, Water Res X 26 (2025), https://doi.org/10.1016/j.wroa.2024.100279.
[22] C. Fritzmann, J. Löwenberg, T. Wintgens, T. Melin, State-of-the-art of reverse osmosis desalination, Desalination 216 (2007) 1–76, https://doi.org/10.1016/j.desal.2006.12.009.

[23] S. Mitrouli, A.J. Karabelas, A. Karanasiou, M. Kostoglou, Incipient calcium carbonate scaling of desalination membranes in narrow channels with spacers-experimental insights, J. Membr. Sci. 425-426 (2013) 48–57, https://doi.org/10.1016/j.memsci.2012.09.025.
[24] T. Waly, M.D. Kennedy, G.J. Witkamp, G. Amy, J.C. Schippers, The role of inorganic ions in the calcium carbonate scaling of seawater reverse osmosis systems, Desalination 284 (2012) 279–287, https://doi.org/10.1016/j.desal.2011.09.012.
[25] C. Tzotzi, T. Pahiadaki, S.G. Yiantsios, A.J. Karabelas, N. Andritsos, A study of CaCO3 scale formation and inhibition in RO and NF membrane processes, J. Membr. Sci. 296 (2007) 171–184, https://doi.org/10.1016/j.memsci.2007.03.031.
[26] M.N. Mangal, V.A. Yangali-Quintanilla, S.G. Salinas-Rodriguez, J. Dusseldorp, B. Blankert, A.J.B. Kemperman, J.C. Schippers, M.D. Kennedy, W.G.J. van der Meer, Application of a smart dosing pump algorithm in identifying real-time optimum dose of antiscalant in reverse osmosis systems, J. Membr. Sci. 658 (2022) 120717, https://doi.org/10.1016/j.memsci.2022.120717.
[27] S. Lee, J. Kim, C.H. Lee, Analysis of CaSO4 scale formation mechanism in various nanofiltration modules, J. Membr. Sci. 163 (1999) 63–74, https://doi.org/10.1016/S0376-7388(99)00156-8.
[28] S.S. Cob, C. Beaupin, B. Hofs, M.M. Nederlof, D.J.H. Harmsen, E.R. Cornelissen, A. Zwijnenburg, F.E.G. Güner, G.J. Witkamp, Silica and silicate precipitation as limiting factors in high-recovery reverse osmosis operations, J. Membr. Sci. 423–424 (2012) 1–10, https://doi.org/10.1016/j.memsci.2012.07.016.
[29] Z. Steiner, H. Rapaport, Y. Oren, R. Kasher, Effect of surface-exposed chemical groups on calcium-phosphate mineralization in water-treatment systems, Environ. Sci. Technol. 44 (2010) 7937–7943, https://doi.org/10.1021/es101773t.
[30] K. Rathinam, A. Modi, D. Schwahn, Y. Oren, R. Kasher, Surface grafting with diverse charged chemical groups mitigates calcium phosphate scaling on reverse osmosis membranes during municipal wastewater desalination, J. Membr. Sci. 647 (2022) 120310, https://doi.org/10.1016/j.memsci.2022.120310.
[31] M.N. Mangal, S.G. Salinas-Rodriguez, V.A. Yangali-Quintanilla, M.D. Kennedy, J.C. Schippers, Chapter 8: Scaling, in: S.G. Salinas-Rodriguez, J.C. Schippers, G. Amy, I. Kim, S., M.D. Kennedy (Eds.) Seawater Reverse Osmosis Desalination: Assessment and Pre-treatment of Fouling and Scaling, IWA, 2021.
[32] J. Rolf, T.C. Cao, X.C. Huang, C. Boo, Q.L. Li, M. Elimelech, Inorganic scaling in Membrane desalination: models, mechanisms, and characterization methods, Environ. Sci. Technol. 56 (2022) 7484–7511, https://doi.org/10.1021/acs.est.2c01858.
[33] DuPont, Filmtec™ reverse osmosis membranes technical manual, 2021.
[34] A. Antony, J.H. Low, S. Gray, A.E. Childress, P. Le-Clech, G. Leslie, Scale formation and control in high pressure membrane water treatment systems: a review, J. Membr. Sci. 383 (2011) 1–16, https://doi.org/10.1016/j.memsci.2011.08.054.
[35] H.J. Oh, Y.K. Choung, S. Lee, J.S. Choi, T.M. Hwang, J.H. Kim, Scale formation in reverse osmosis desalination: model development, Desalination 238 (2009) 333–346, https://doi.org/10.1016/j.desal.2008.10.005.
[36] L. Boels, Removal and recovery of phosphonate antiscalants, mechanical, maritime and materials engineering, Delft University of Technology, Delft, the Netherlands, 2012. PhD (thesis.), 2012.
[37] L.F. Greenlee, F. Testa, D.F. Lawler, B.D. Freeman, P. Moulin, The effect of antiscalant addition on calcium carbonate precipitation for a simplified synthetic brackish water reverse osmosis concentrate, Water Res. 44 (2010) 2957–2969, https://doi.org/10.1016/j.watres.2010.02.024.
[38] R. Kuhn, C. Vornholt, V. Preuss, I.M. Bryant, M. Martienssen, Aminophosphonates in Nanofiltration and reverse osmosis permeates, Membranes-Basel 11 (2021), https://doi.org/10.3390/membranes11060446.
[39] A. Sweity, Y. Oren, Z. Ronen, M. Herzberg, The influence of antiscalants on biofouling of RO membranes in seawater desalination, Water Res. 47 (2013) 3389–3398, https://doi.org/10.1016/j.watres.2013.03.042.
[40] G. Hasanin, A.M. Mosquera, A.H. Emwas, T. Altmann, R. Das, P.J. Buijs, J. S. Vrouwenvelder, G. Gonzalez-Gil, The microbial growth potential of antiscalants used in seawater desalination, Water Res. 233 (2023), https://doi.org/10.1016/j.watres.2023.119802.
[41] M.N. Mangal, S.G. Salinas-Rodriguez, J. Dusseldorp, B. Blankert, V.A. Yangali-Quintanilla, A.J.B. Kemperman, J.C. Schippers, W.G.J. van der Meer, M. D. Kennedy, Foulant identification and performance evaluation of antiscalants in increasing the recovery of a reverse osmosis system treating anaerobic groundwater, Membranes-Basel 12 (3) (2022) 290, https://doi.org/10.3390/membranes12030290.
[42] M. Futterlieb, I.A.M. ElSherbiny, M. Tuczinski, J. Lipnizki, S. Panglisch, Limits of high recovery inland desalination: closed-circuit reverse osmosis - a viable option? Chem. Ing. Tech. 93 (2021) 1359–1368, https://doi.org/10.1002/cite.202100042.
[43] M. Vanoppen, G. Stoffels, J. Buffel, B. De Gusseme, A.R.D. Verliefde, A hybrid IEX-RO process with brine recycling for increased RO recovery without chemical addition: a pilot-scale study, Desalination 394 (2016) 185–194, https://doi.org/10.1016/j.desal.2016.05.003.
[44] P. Nativ, L. Birnhack, O. Lahav, A new pretreatment approach for applying high-recovery reverse osmosis desalination to highly scaling brackish groundwater, Desalination 564 (2023), https://doi.org/10.1016/j.desal.2023.116778.
[45] G.M. Ayoub, R.M. Zayyat, M. Al-Hindi, Precipitation softening: a pretreatment process for seawater desalination, Environ. Sci. Pollut. R. 21 (2014) 2876–2887, https://doi.org/10.1007/s11356-013-2237-1.
[46] S.H. Maruf, A.R. Greenberg, J. Pellegrino, Y.F. Ding, Fabrication and characterization of a surface-patterned thin film composite membrane, J. Membr. Sci. 452 (2014) 11–19, https://doi.org/10.1016/j.memsci.2013.10.017.
[47] X.C. Huang, C. Li, K.C. Zuo, Q.L. Li, Predominant effect of material surface hydrophobicity on gypsum scale formation, Environ. Sci. Technol. 54 (2020) 15395–15404, https://doi.org/10.1021/acs.est.0c03826.
[48] E. Hosseinipour, E. Harris, H.A. El Nazer, Y.M.A. Mohamed, P.A. Davies, Desalination by batch reverse osmosis (RO) of brackish groundwater containing sparingly soluble salts, Desalination 566 (2023), https://doi.org/10.1016/j.desal.2023.116875.
[49] D.M. Warsinger, E.W. Tow, L.A. Maswadeh, G.B. Connors, J. Swaminathan, V.J. H. Lienhard, Inorganic fouling mitigation by salinity cycling in batch reverse osmosis, Water Res. 137 (2018) 384–394, https://doi.org/10.1016/j.watres.2018.01.060.
[50] N. Pomerantz, Y. Ladizhansky, E. Korin, M. Waisman, N. Daltrophe, J. Gilron, Prevention of scaling of reverse osmosis membranes by “zeroing” the elapsed nucleation time. Part I. Calcium sulfate, Ind. Eng. Chem. Res. (2006), https://doi.org/10.1021/ie051040k.
[51] Y.A. Jarma, Y. Kim, Y. Cohen, Reverse osmosis desalination combining feed flow reversal with permeate flush for mitigation of mineral scaling, Desalination 574 (2024) 117273, https://doi.org/10.1016/j.desal.2023.117273.
[52] H. Gu, M.H. Plumlee, M. Li, A. Mohseni, R. Erlitzki, Enhancing municipal potable reuse recovery with flow-reversal RO: pilot study, challenges, and retrofit considerations, Desalination 601 (2025) 118594, https://doi.org/10.1016/j.desal.2025.118594.
[53] Z.X. Hu, A. Antony, G. Leslie, P. Le-Clech, Real-time monitoring of scale formation in reverse osmosis using electrical impedance spectroscopy, J. Membr. Sci. 453 (2014) 320–327, https://doi.org/10.1016/j.memsci.2013.11.014.
[54] A. Antony, T. Chilcott, H. Coster, G. Leslie, In situ structural and functional characterization of reverse osmosis membranes using electrical impedance spectroscopy, J. Membr. Sci. 425 (2013) 89–97, https://doi.org/10.1016/j.memsci.2012.09.028.
[55] K.D. Cobry, Z. Yuan, J. Gilron, V.M. Bright, W.B. Krantz, A.R. Greenberg, Comprehensive experimental studies of early-stage membrane scaling during nanofiltration, Desalination 283 (2011) 40–51, https://doi.org/10.1016/j.desal.2011.04.053.
[56] A.R. Bartman, E. Lyster, R. Rallo, P.D. Christofides, Y. Cohen, Mineral scale monitoring for reverse osmosis desalination via real-time membrane surface image analysis, Desalination 273 (2011) 64–71, https://doi.org/10.1016/j.desal.2010.10.021.
[57] M. Uchymiak, A. Rahardianto, E. Lyster, J. Glater, Y. Cohen, A novel RO ex situ scale observation detector (EXSOD) for mineral scale characterization and early detection, J. Membr. Sci. 291 (2007) 86–95, https://doi.org/10.1016/j.memsci.2006.12.038.
[58] O.D. Supekar, J.J. Brown, A.R. Greenberg, J.T. Gopinath, V.M. Bright, Real-time detection of reverse-osmosis Membrane scaling via Raman spectroscopy, Ind. Eng. Chem. Res. 57 (2018) 16021–16026, https://doi.org/10.1021/acs.iecr.8b01272.
[59] O.D. Supekar, D.J. Park, A.R. Greenberg, J.T. Gopinath, V.M. Bright, Real-time detection of early-stage calcium sulfate and calcium carbonate scaling using raman spectroscopy, J. Membr. Sci. 596 (2020) 117603, https://doi.org/10.1016/j.memsci.2019.117603.
[60] M. Uchymiak, A.R. Bartman, N. Daltrophe, M. Weissman, J. Gilron, P. D. Christofides, W.J. Kaiser, Y. Cohen, Brackish water reverse osmosis (BWRO) operation in feed flow reversal mode using an ex situ scale observation detector (EXSOD), J. Membr. Sci. 341 (2009) 60–66, https://doi.org/10.1016/j.memsci.2009.05.039.
[61] D.J. Park, O.D. Supekar, V.M. Bright, A.R. Greenberg, J.T. Gopinath, Raman spectroscopy for real-time concurrent detection of multiple scalants on RO membranes, Desalination 565 (2023), https://doi.org/10.1016/j.desal.2023.116851.
[62] C.A.C. van de Lisdonk, J.A.M. van Paassen, J.C. Schippers, Monitoring scaling in nanofiltration and reverse osmosis membrane systems, Desalination 132 (2000) 101–108, https://doi.org/10.1016/S0011-9164(00)00139-9.
[63] E.G. Darton, Membrane chemical research: centuries apart, Desalination 132 (2000) 121–131, https://doi.org/10.1016/S0011-9164(00)00141-7.
[64] Stumm, W., Morgan, J.J. Aquatic chemistry. 3 ed. 1996.
[65] A.G. Reiss, I. Gavrieli, Y.O. Rosenberg, I.J. Reznik, A. Luttge, S. Emmanuel, J. Ganor, Gypsum precipitation under saline conditions: thermodynamics, kinetics, morphology, and size distribution, Minerals-Basel 11 (2021), https://doi.org/10.3390/min11020141.
[66] D.L. Parkhurst, C.A.J. Appelo, Description of input and examples for PHREEQC version 3 — a computer program for speciation, batch-reaction, one-dimensional transport, and inverse geochemical calculations., 2013.
[67] Markov, I.V. Crystal growth for beginners: fundamentals of nucleation. Crystal Growth and Epitaxy. 1995.
[68] A.G. Pervov, Scale formation prognosis and cleaning procedure schedules in reverse-osmosis systems operation, Desalination 83 (1991) 77–118, https://doi.org/10.1016/0011-9164(91)85087-B.
[69] M. Qasim, M. Badrelzaman, N.N. Darwish, N.A. Darwish, N. Hilal, Reverse osmosis desalination: a state-of-the-art review, Desalination 459 (2019) 59–104, https://doi.org/10.1016/j.desal.2019.02.008.
[70] A. Matin, F. Rahman, H.Z. Shafi, S.M. Zubair, Scaling of reverse osmosis membranes used in water desalination: phenomena, impact, and control; future directions, Desalination 455 (2019) 135–157, https://doi.org/10.1016/j.desal.2018.12.009.
[71] S.F.E. Boerlage, M.D. Kennedy, I. Bremere, G.J. Witkamp, J.P. van der Hoek, J. C. Schippers, Stable barium sulphate supersaturation in reverse osmosis, J. Membr. Sci. 179 (2000) 53–68, https://doi.org/10.1016/S0376-7388(00)00504-4.

[72] O. Sohnel, J.W. Mullin, Precipitation of calcium-carbonate, J. Cryst. Growth 60 (1982) 239–250, https://doi.org/10.1016/0022-0248(82)90095-1.
[73] O. Söhnel, J. Garside, Precipitation: baisc principes and industrial applications, 1992.
[74] N. Dhakal, S.G. Salinas Rodriguez, J.C. Schippers, M.D. Kennedy, Induction time measurements in two brackish water reverse osmosis plants for calcium carbonate precipitation, Desalin. Water Treat. 53 (2015) 285–293, https://doi.org/10.1080/19443994.2014.903870.
[75] S.X. Jiang, Y.N. Li, B.P. Ladewig, A review of reverse osmosis membrane fouling and control strategies, Sci. Total Environ. 595 (2017) 567–583, https://doi.org/10.1016/j.scitotenv.2017.03.235.
[76] M.K. Shahid, M. Pyo, Y.G. Choi, Carbonate scale reduction in reverse osmosis membrane by CO2 in wastewater reclamation, Membr. Water Treat. 8 (2017) 125–136, https://doi.org/10.12989/mwt.2017.8.2.125.
[77] SWDU. Stadtwerke Duisburg Trinkwasseranalyse. 2024 25th of September 2024]; Available from: https://www.stadtwerke-duisburg.de/privatkunden/themen/trinkwasser.
[78] Suez. AK P Series RO Membrane Elements. 2024 28th of August 2024]; Available from: https://www.watertechnologies.com/sites/default/files/documents/CB_AKP_Series_EN_v2_0.pdf.
[79] Lenntech. Low Energy Brackish Water RO, Elements (2024), 26th of September 2024]; Available from: https://www.lenntech.com/Data-sheets/Veolia-AK-series-EN-L.pdf.
[80] DuPont. FilmTec™ XLE PRO-4040 & XLE PRO-2540. 2024 26th of September 2024]; Available from: https://www.dupont.com/content/dam/dupont/amer/us/en/water-solutions/public/documents/en/RO-FilmTec-XLE-PRO-4040-and-XLE-PRO-2540-PDS-45-D03972-en.pdf.
[81] DuPont. FilmTec™ BW30 PRO-4040 & BW30 PRO-2540. 2024 26th of September 2024]; Available from: https://www.dupont.com/content/dam/dupont/amer/us/en/water-solutions/public/documents/en/RO-FilmTec-BW30-PRO-4040-and-BW30-PRO-2540-PDS-45-D03970-en.pdf.
[82] J.S. Vrouwenvelder, C. Hinrichs, W.G.J. van der Meer, M.C.M. van Loosdrecht, J. C. Kruithof, Pressure drop increase by biofilm accumulation in spiral wound RO and NF membrane systems: role of substrate concentration, flow velocity, substrate load and flow direction, Biofouling (2009), https://doi.org/10.1080/08927010902972225.
[83] D. Szpak, B. Tchorzewska-Cieslak, K. Pietrucha-Urbanik, Analysis of the turbidity of raw water in the context of water-supply safety, Desalin. Water Treat. 186 (2020) 281–289, https://doi.org/10.5004/dwt.2020.25176.
[84] H.C. Flemming, Biofouling Bei Membranprozessen, Springer, 1995.
[85] M. Herzberg, M. Elimelech, Biofouling of reverse osmosis membranes: role of biofilm-enhanced osmotic pressure, J. Membr. Sci. 295 (2007) 11–20, https://doi.org/10.1016/j.memsci.2007.02.024.
[86] E.M.V. Hoek, M. Elimelech, Cake-enhanced concentration polarization: a new fouling mechanism for salt-rejecting membranes, Environ. Sci. Technol. 37 (2003) 5581–5588, https://doi.org/10.1021/es0262636.
[87] J. Thompson, N. Lin, E. Lyster, R. Arbel, T. Knoell, J. Gilron, Y. Cohen, RO membrane mineral scaling in the presence of a biofilm, J. Membr. Sci. 415 (2012) 181–191, https://doi.org/10.1016/j.memsci.2012.04.051.
[88] M.N. Mangal, S.G. Salinas-Rodriguez, B. Blankert, V.A. Yangali-Quintanilla, J. C. Schippers, W.G.J. van der Meer, M.D. Kennedy, Role of phosphate and humic substances in controlling calcium carbonate scaling in a groundwater reverse osmosis system, J. Environ. Chem. Eng. 9 (2021), https://doi.org/10.1016/j.jece.2021.105651.
[89] E. Curcio, X.S. Ji, G. Di Profio, A. Sulaiman, E. Fontananova, E. Drioli, Membrane distillation operated at high seawater concentration factors: role of the membrane on CaCO3 scaling in presence of humic acid, J. Membr. Sci. 346 (2010) 263–269, https://doi.org/10.1016/j.memsci.2009.09.044.
[90] A.R. Hoch, M.M. Reddy, G.R. Aiken, Calcite crystal growth inhibition by humic substances with emphasis on hydrophobic acids from the Florida everglades, Geochim. Cosmochim. Acta 64 (2000) 61–72, https://doi.org/10.1016/S0016-7037(99)00179-9.
[91] M. Kellermeier, A. Picker, A. Kempter, H. Cölfen, D. Gebauer, A straightforward treatment of activity in aqueous CaCO3 solutions and the consequences for nucleation theory, Adv. Mater. 26 (2014) 752–757, https://doi.org/10.1002/adma.201303643.
[92] Y. Zarga, H. Ben Boubaker, N. Ghaffour, H. Elfil, Study of calcium carbonate and sulfate co-precipitation, Chem. Eng. Sci. 96 (2013) 33–41, https://doi.org/10.1016/j.ces.2013.03.028.
[93] W.D. Li, X. Su, A. Palazzolo, S. Ahmed, E. Thomas, Reverse osmosis membrane, seawater desalination with vibration assisted reduced inorganic fouling, Desalination 417 (2017) 102–114, https://doi.org/10.1016/j.desal.2017.05.016.
[94] S. Cespedes, F.D. Martinez, F. Salto-Quintana, B. Blankert, C. Picioreanu, Three-dimensional concentration-polarization modeling of trace-ions in reverse osmosis, J. Membr. Sci. 693 (2024) 122349, https://doi.org/10.1016/j.memsci.2023.122349.
[95] K. Onuma, A. Oyane, T. Kokubo, G. Treboux, N. Kanzaki, A. Ito, Nucleation of calcium phosphate on 11-mercaptoundecanoic acid self-assembled monolayer in a pseudophysiological solution, J. Phys. Chem. B 104 (2000) 11950–11956, https://doi.org/10.1021/jp002015p.